ELSEVIER

Polymer 43 (2002) 4011–4016

polymer

www.elsevier.com/locate/polymer

Space charge and internal electric field distribution in poly(2,5-pyridinediyl)

F. Feller[a,*], D. Geschke[a], A.P. Monkman[b]

[a]*Gruppe Polymerphysik, Institut für Experimentelle Physik I, Universität Leipzig, Linnéstrasse 5, D-04103 Leipzig, Germany*
[b]*Organic Electroactive Materials Research Group, Department of Physics, University of Durham, South Road, Durham DH1 3LE, UK*

Received 25 October 2001; received in revised form 7 March 2002; accepted 22 March 2002

Abstract

We present measurements of the spatial distribution of space charge and the internal electric field in 3–4 μm thick films of a luminescent conjugated polymer by means of the laser intensity modulation method. The internal electric field is spatially modified by the existence and persistence of space charge layers induced by the external bias. We observe a double layer of homo-charges and hetero-charges, which is explained by a trapping model that implements the presence of traps near the surface of the film. Within this model, space charge layers are built up by a combination of carrier injection from the electrodes, not into the valence or conduction bands, but directly into intra-gap traps near the interface, as well as the separation of bulk electrons and holes in the external field and subsequent trapping. A trap density of about 10^{23} m^{-3} is concluded from the results. In addition, the conjugated polymer poly(2,5-pyridinediyl) is found to have strong electret properties with local charge storage of up to 500 C/m^3.

Keywords: Conjugated polymers; Space charge; Trapping

1. Introduction

During the last decade, conjugated polymers have attracted scientific interest because of their semi-conducting properties, especially they have been demonstrated as prototypes for applications in the field of LEDs and display systems. In the basic thin film device, a polymer light emitting diode (PLED), electroluminescence (EL) arises through the radiative recombination of electron–hole pairs in those materials. The rate of this recombination and therewith the EL-efficiency depends on the amount of mobile electrons and holes, as well as on the presence of traps, i.e. impurities or lattice defects in the material. In the trap free case, the current across a conjugated polymer film is determined by the interplay between the carrier injection process [1,2] at the electrodes and the hopping transport of charge carriers in the bulk of the film [3,4]. Depending on the height of the injection barrier between the electrode metal work function and the corresponding transport level in the polymer, the current in the device is dominated by either of two mechanisms. In an ideal electrode configuration, the electrode work functions are matched to the polymer electron and hole transport levels resulting in very small injection barriers and conduction, that is, limited by transport within the bulk. This leads to the accumulation of excess charge carriers close to the injecting contact, which form a space charge layer that distorts the internal electric field, the current becomes space charge limited [5]. A second mechanism for the accumulation of space charge is deep trapping of charge carriers at extrinsic or intrinsic defects, which should always be present in real polymers. Thus, in order to improve the performance of conjugated polymer devices, it is of particular importance to understand the phenomena of space charge accumulation in thin films. In this respect, measurements of space charge limited conduction (SCLC) have been performed by fitting current–voltage data to several SCLC-models implying different trap energy distributions [6,7]. In addition, deep level transient spectroscopy (DLTS) and impedance measurements of the space charge capacity of the metal–polymer contact have been performed to measure trap densities and energies [8–10].

In this work, we present results of spatially resolved electric field and space charge measurements in a conjugated polymer obtained using the laser intensity modulation method (LIMM). We have recently demonstrated the application of this method for the investigation of space charges in conjugated polymer films of several micrometer thickness [11]. Since the development of LIMM by Lang and Das-Gupta [12], it has mainly been used to study the

* Corresponding author.
E-mail address: feller@physik.uni-leipzig.de (F. Feller).

0032-3861/02/$ - see front matter
PII: S0032-3861(02)00228-8

depth profile of the polarisation distribution in thin ferroelectric films [13,14], as well as space charge distributions in poled electret films [15,16].

Our measurements were performed on the conjugated polymer poly(2,5-pyridinediyl) (PPY), a promising electron transporting polymer for applications in light emitting diodes [17,18]. We will demonstrate the charge storing properties of PPY and investigate the influence of the space charge layers on the internal electric field.

2. Experimental

PPY was synthesised as described previously [17] and dissolved in formic acid using a concentration of 30 mg/ml. Films 3–5 μm thick were prepared by spin-casting or drop-casting from solution onto gold covered glass substrates and subsequent evaporation of a second gold electrode (front electrode). The front electrode was covered by an additional 20 nm bismuth layer to enhance absorption of the laser light. The LIMM experiment is explained in more detail elsewhere [14] and only briefly described here. The set-up consists of a HeNe laser, it is beam being intensity-modulated by an acousto-optical modulator with a frequency f supplied by a frequency generator (Fig. 1). The sample itself is mounted onto a heat sink and fixed with silver paint to ensure good thermal contact between the substrate and the metal of the sink. The pyroelectric response of the sample is detected as a small AC current between the gold electrodes. This pyrocurrent is amplified by a current-to-voltage converter (CVC) using a gain of 10^5 V/A and measured by a lock-in amplifier with the reference frequency matched to the frequency generator that provides the modulation frequency f for the acousto-optic modulator. In addition, a galvanic decoupling unit has been used to allow the application of a DC bias during the very sensitive AC current measurements across the same electrodes. The frequency sweep of the frequency generator and the data recording is controlled by a computer.

In order to increase the resolution of the method in films only a few micrometers thick the electronic components have been modified to extend the frequency region beyond 100 kHz. A special designed CVC is used in combination with a EG&G 5302 lock-in amplifier allowing measurements up to 600 MHz, which corresponds to a minimal measurement depth of 200 nm.

3. Theory of LIMM

When the modulated laser beam hits the front electrode of the sample, it is absorbed and transformed into a heat wave that penetrates into the sample. Since the front electrode is opaque, no light is transmitted to the polymer. In addition, laser light reaching the film via reflection or scattering effects do not lead to excitation, since the laser wavelength (632 nm) is far away from any absorption bands of the polymer. Depending on the modulation frequency f of the incident laser beam and on certain thermal parameters of the material, the heat wave establishes a dynamic temperature profile with respect to the coordinate z along the film normal [15]:

$$T(f,z) = \frac{q_0}{\kappa K} \frac{\cosh[K(L-z)] + a_L \sinh[K(L-z)]}{(a_0 + a_L)\cosh(KL) + [1 + a_L a_0]\sinh(KL)} \tag{1}$$

Therein q_0 denotes the total amount of heat absorbed by the top electrode, κ is for the thermal conductivity of the material, a_0 and a_L are the heat transfer coefficients at the top and the bottom electrode, respectively, the complex $K = (1 + i)\sqrt{(\pi f/\chi)}$ is the wave number of the thermal waves, which can be inferred from the modulation frequency f of the laser beam and the thermal diffusivity χ of the material. Approximately, the real part of the complex temperature distribution produced in the polymer film at a certain modulation frequency f can be understood as a continuously falling function with maximum at $z = 0$ (at the front electrode) vanishing at the *heat wave penetration depth* $\sigma_f = \sqrt{\chi/\pi f}$.

For a certain modulation frequency f, the complex amplitude of the pyroelectric current $I_P(f)$ in a film of thickness L and illuminated area A is well described by the fundamental LIMM equation [12]:

$$I_P(f) = 2\pi i f \frac{A}{L} \int_0^L r(z) T(f,z)\, \mathrm{d}z \tag{2}$$

$r(z)$ is the desired distribution function, which in non-polar materials has only contributions from space charges $\rho(z)$ and the externally applied electric field $E_{ext}(z)$:

$$r(z) = (\alpha_\chi - \alpha_\varepsilon)\varepsilon_0 \varepsilon (E_\rho(z) + E_{ext}(z))$$

with

$$\varepsilon_0 \varepsilon E_\rho(z) = R(z) - \frac{1}{L}\int_0^L R(y)\,\mathrm{d}y, \qquad R(z) = \int_0^z \rho(\xi)\,\mathrm{d}\xi \tag{3}$$

where α_χ and α_ε denote the thermal coefficients of expansion and dielectric permittivity, respectively. In the LIMM experiment, the pyroelectric current $I_P(f)$ is measured as a function of the modulation frequency f. Afterwards, the distribution function $r(z)$ has to be inferred via inversion of the integral equation (Eq. (2)) using the temperature profile $T(f,z)$ (Eq. (1)), that is, calculated for the specific thermal parameters. This is, however, known to be an ill-posed inverse problem, since the distribution function $r(z)$ does not depend continuously upon the LIMM data [19]. Accordingly, small aberrations in the data, which are inevitably affected by measurement errors, will result in large or even unbounded errors of the reconstructed distribution function $r(z)$. In order to solve such ill-posed inverse problems special mathematical methods, i.e. regularisation methods, are necessary [20,21]. We have recently improved the standard regularisation method by introducing a more adequate regularisation term and a more realistic error

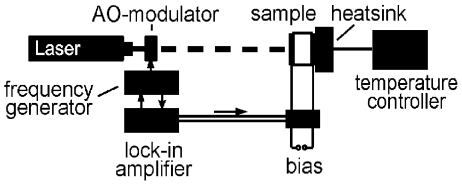

Fig. 1. Experimental set-up of the LIMM.

model [22]. With respect to the particular importance of the analysis in the region close to the front electrode we have also applied an analysis from Ploss and co-workers based on a high frequency approximation of the temperature distribution $T(f,z)$ [23,24].

4. Results

A 4 μm thick Au/PPY/Au device was biased using a DC applied field of 7.5 MV/m. Fig. 2 shows the temporal development of the pyroelectric response of the sample to the switching-on of the applied bias. The signal was found to increase over several minutes until it approached it is final value. The same retarded response was observed for every change in the applied bias. Therefore, after each bias change, the sample was allowed to settle for 30 min before starting the measurements. The LIMM spectrum is depicted in Fig. 3. Every data point is obtained by averaging 100 current readings from the lock-in. Because of the long time to record a spectrum, the different frequency points were triggered in random order to detect systematic drifts of the signal due to chemical reactions/degeneration, etc. The real part of the pyrocurrent has a maximum at about 30 kHz and decreases at lower frequencies. At higher frequencies, the pyrocurrent rapidly decreases and becomes negative forming a negative peak at about 400 kHz. In Fig. 4, the real parts of two LIMM spectra recorded for a sample under an electric field of +5 and −5 MV/m are depicted. It shows that the pyroelectric current changes

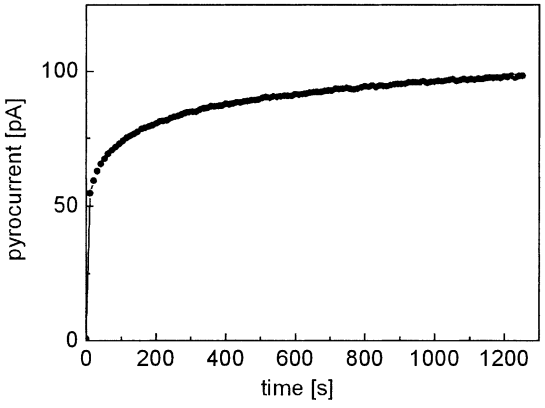

Fig. 2. The pyroelectric current of a 4 μm thick Au/PPY/Au device as a function of time recorded after the application of an external field of 12 MV/m at the time $t = 0$. The modulation frequency was $f = 10$ kHz.

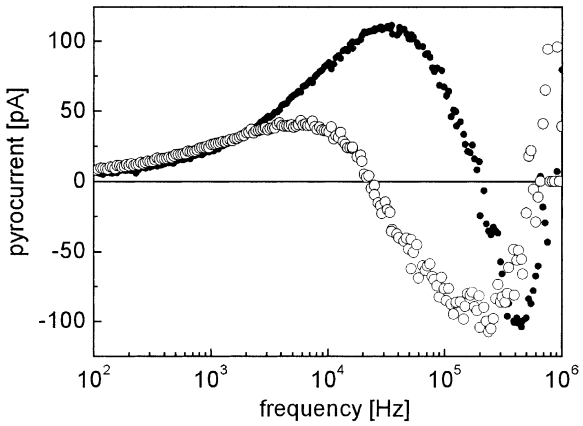

Fig. 3. The LIMM spectrum of a 4 μm thick Au/PPY/Au device represented by it is real part (filled symbols) and it is imaginary part (open symbols). The externally applied electric field was 7.5 MV/m.

sign with the applied field and the whole LIMM spectrum is very symmetric with respect to the applied bias.

Fig. 5 shows the distribution of the electric field along the film normal z. The upper curve is the result of the regularisation, while the lower one is obtained using the approximation after Ploss et al. [23]. Both curves indicate the electric field to vanish at the electrode and show a strong peak at about 600 nm. At the maximum, the local internal field exceeds the externally applied field of 7.5 MV/m. On the other hand, in the bulk of the sample, beyond 1 μm the field is reduced significantly. In the solution of the regularisation, the field is even turning negative at some positions. Those turnings around the base line before and after the main feature are typically observed in solutions of regularisation programs and attributed to numerical artefacts [22].

As another difference between the two solutions, the approximated distribution has a higher magnitude than the result of the regularisation. A more detailed study of the regularisation process using simulated LIMM-data from given distributions shows that the spatial resolution

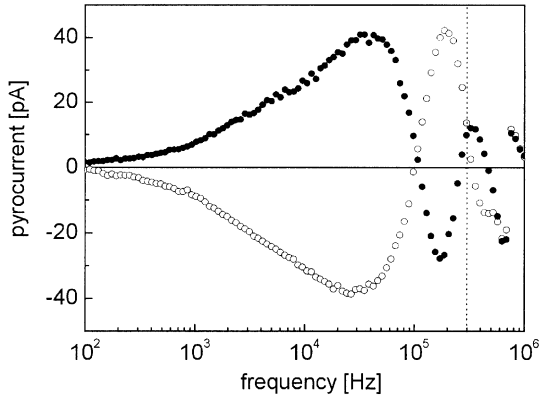

Fig. 4. LIMM spectra of a 4 μm thick Au/PPY/Au device using different directions of the applied electric field (+5 and −5 MV/m, respectively). Spectra have been recorded after 20 min settling time because of the slow pyroelectric response of the samples to a change in bias.

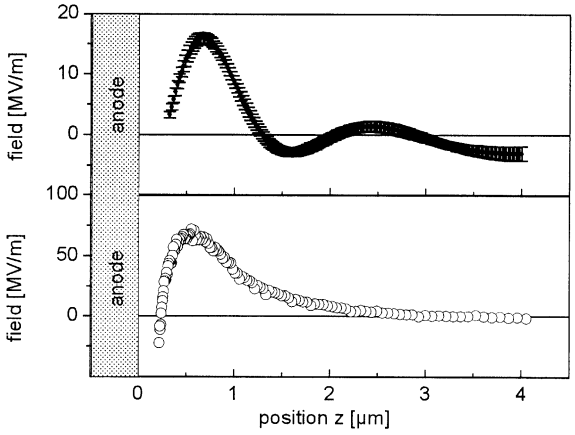

Fig. 5. The distribution of the internal electric field obtained via Eq. (2) from the LIMM spectrum in Fig. 3. The upper curve represents the result of the regularisation as described in Ref. [21,22], while the lower curve is obtained using an approximation of the temperature distribution at high frequencies [23,24].

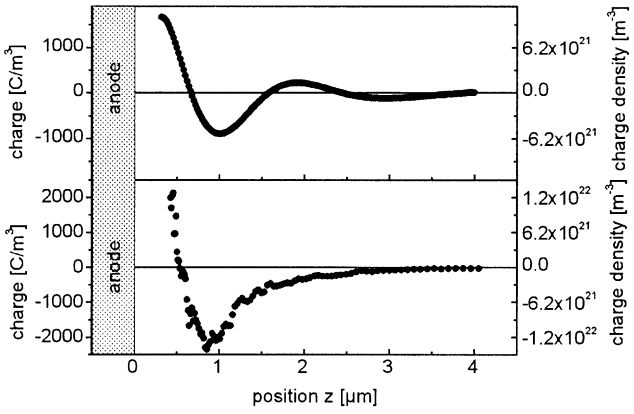

Fig. 6. Space charge distribution in a 4 μm thick Au/PPY/Au device obtained from the distribution of the internal electric field via Eq. (3). Again, the upper and lower curves are the results of regularisation and approximation, respectively. The approximated solution for the electric field distribution was submitted to a 15 points smoothing procedure before taking the derivative (lower curve).

of narrow peaks is limited by a natural line width (NLW) and that the existence of narrower features in the 'true' distribution results in a broadening and flattening of the solution [22]. Since the main peak at about 500 nm in the approximation is relatively broad, the flattening of the regularised solution might be due to the strong rise of the signal near the front electrode.

In addition, in every LIMM experiment there is, a priori, increasing uncertainty of the data for deeper parts of the sample near the rear side of the electrode. This region is calculated from the lower frequency part of the LIMM spectrum. At low frequencies, the laser-induced temperature gradient across the sample is very weak, which decreases the spatial resolution of the method. To achieve information about the distribution near the back electrode, it is therefore necessary to carry out a second measurement illuminating the sample through the glass substrate on the back of the film [11]. In our films, it was observed that the pyroelectric response is significantly reduced by more than an order of magnitude, when the sample was illuminated through the back electrode, indicating a similar, but much weaker distribution near the back side of the film.

From the distribution of the electric field, the spatially resolved space charge profile can be derived via Eq. (3). Fig. 6 shows the space charge distributions in the Au/PPY/Au device, obtained from both, regularised and approximated solution. Originating from the difference in the electric field data, the lower curve, obtained via approximation, is bigger by a factor of two compared to the upper curve, obtained via regularisation. Both curves show a strong homo-charge layer near the anode up to about 500 nm followed by a negatively charged layer (hetero-charges) of similar extent.

From this results alone, it is difficult to decide whether the narrow positive feature from $z = 0.500$ nm originates from a real homo-charge layer in the polymer next to the electrode or if it is the charge at the electrode itself, that is, broaden by the analysis, especially when keeping in mind the minimum penetration depth of the experiment of about 200–300 nm. However, this can be ruled out by comparing the field and space charge distribution of a biased and a short-circuited sample (Fig. 7). It turns out that in the latter case, where the electrodes do not carry any charges a similar distribution is observed, only reduced in magnitude by a factor of about 15. Therefore, the observed distribution near the electrode must originate from a charged layer within the polymer.

Comparing the two methods for analysing LIMM data on relatively thin films, it is found that they both yield similar results. The regularisation calculates very smooth results and provides error assessment, but tends to produce slightly broadened and too low distributions, when resolving narrow

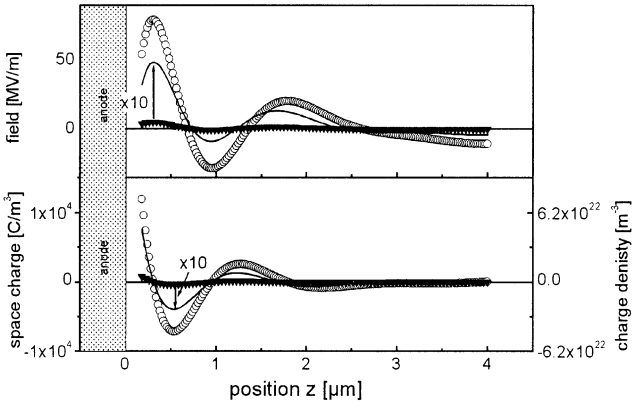

Fig. 7. Charge storage in PPY. Electric field (upper curves) and space charge distributions (lower curves) in PPY. The open symbols represent the results of the device under bias, while the filled symbols show the distributions, when the sample is short-circuited (zero bias). For better visibility, the 10 times enlarged zero-bias distributions are also depicted as solid lines, demonstrating the constancy in shape.

charge layers. On the other hand, the approximation method is very easy to use and produces reliable results, but the solutions are noisy and need to be smoothed before the derivative (space charge distribution) can be calculated. All in all, the results of the approximation are preferred for the analysis of thin film LIMM-data because of the higher resolution near the front electrode.

5. Discussion

In conjugated polymers, charge carrier balance is determined by the coexistence of injection of extrinsic carriers from the electrodes and transport of bulk charge carriers. Transport of charge carriers is realised by hopping of electrons or holes between different sites, i.e. polymer chains, in an external electric field. This process implies the existence of electrons/holes with an adequate energy near the conduction/valence band, respectively. In PLEDs, those carriers are directly provided by the injecting electrode, when the electrode work function matches the corresponding transport levels in the polymer. In our Au/PPY/Au devices, the barrier heights are 1.8 eV for electrons and 1.1 eV for holes [25]. Thus, injection of mobile carriers is strongly hindered, which results in very low DC currents, always below 10 nA, when the sample is biased (Fig. 8).

With this in mind, we propose the following model to explain the observed charge layers in our devices. We assume at this point the front electrode to be positively charged. The two main features observed in the space charge distribution, the positively charged layer near the front electrode and the adjacent negatively charged layer are induced by two separate processes: the first process involves the injection of holes. Because of the high injection, barrier holes cannot efficiently be injected into the valence band, but in the presence of deep traps near the surface holes can be directly transferred from the anode into these trapping sites inside the polymer. Traps arising from chemical defects will be electrically neutral in the macroscopic lattice and the accumulation of trapped holes leads to a build-up of positive space charge. This space charge, consequentially, can only slowly follow changes of the external field because of the very low mobility of deeply trapped carriers. This explains the observed response times in the range of minutes, when the polarity of the bias is inverted and the remnant pyrosignal after short-circuiting the devices. Experiments are in progress investigating the temporal development of the pyrosignal in more detail.

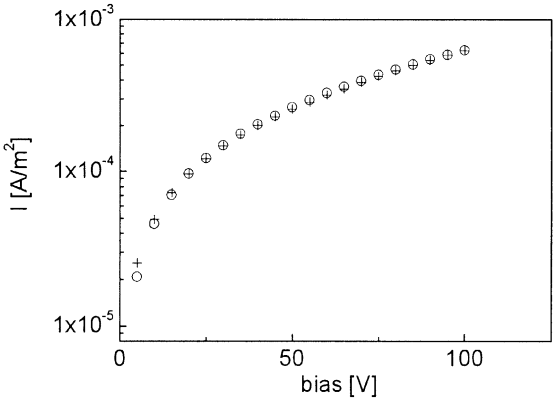

Fig. 8. Current–voltage curve of a typical 4 μm thick Au/PPY/Au device in forward (circles) and reverse bias (crosses). The current is 4–5 orders of magnitude smaller than typical currents in low barrier polymer devices. Assuming space charge limited transport or Ohmic transport in the bulk with $I_{SCLC} \propto (V^2/L^3) = F^2/L$ or $I_\Omega \propto F$ the high thickness of the PPY devices can only account for a current decrease of at the most one order of magnitude (for SCLC). This demonstrates the effect of the high barrier in Au/PPY/Au devices to prevent injection of mobile electrons or holes.

A second process is responsible for the smaller negative feature in Fig. 6. In every conjugated polymer film, there is a certain amount of charge arising from accidental doping, i.e. dopants introduced through the synthesis and the solvent. The charge can then be transported by polarons or charge transfer between neighbouring chains. This allows movement and redistribution of charge within the film following the external applied bias. The charge profile across the sample should be determined by a charge separation process. Positive charges travel towards the cathode and negative charges move towards the anode. Near the anode, negative charges can be either trapped in the trapping zone near the electrode or they can traverse this trapping zone and be captured by the electrode or they can recombine with trapped holes. Trapped negative charge shields the external field and prevents further charge separation. In analogy to the deeply trapped (injected) holes, the pyroelectric response of the negative space charge layer is also very slow and allows the storage of charge after removing the external field. Therefore, the observed double space charge layer and the long pyroelectric response times can be explained by the superposition of the charge distributions of both processes, injection of carriers into deep traps near the surface and charge separation in the bulk. After removing the bias, the deeply trapped carriers cannot flow back to equalise the charge distribution and to compensate the charge layers completely. Therefore, a residual charge profile with the same shape remains at zero bias (Fig. 7).

The symmetry in shape and magnitude of the LIMM spectrum with respect to the externally applied electric field indicates equal capabilities of the material to store either positive or negative charges. This does, however, not necessarily imply equal mobility of electrons and holes for two reasons: first, the LIMM spectra are taken at equilibrium after a sufficient poling time to allow the filling/emptying of the deep traps. Different mobilities would influence the dynamics of the repolarisation process, i.e. switching time, rather than the total amount of accumulated charge after a sufficiently long time. Second, carrier mobilities as measured in time-of-flight or photo-current measurements relate to electrons and holes within the transport level, while the observed space charge distribution is also influenced by injection into trapping levels and charge transfer between

traps as described earlier. Since the response times of mobile carriers in conjugated polymers are very short (<1 ms compared to the time resolution of pyroelectric measurements of about 1 s), it is not possible to investigate the dynamics of charge carriers within the transport levels using LIMM. The observed symmetric switching of the LIMM spectrum with applied bias is therefore indicative of the coexistence of both, donator and acceptor traps.

In Fig. 6, we have provided absolute values for the space charge density at each position in the film. In particular, we obtain a density of trapped carriers very close to the electrode of about 10^{22} m^{-3}. For more intense poling (>25 MV/m up to electrical breakdown), this number increases up to 10^{23} m^{-3}, which suggests that this number corresponds to the absolute trap density. This can be compared with results of DLTS measurements on ITO/PPV/Al devices (200 nm) [6,8]. These investigations involved capacitance measurements of the Schottky contact, yielding values for the total hole trap density of 4×10^{22} and 5×10^{23} m^{-3} in PPV. A value of a few times 10^{22} m^{-3} was also reported from impedance measurements on similar structures [10]. On the other hand, comparing the space charge densities with non-conjugated polymers (common insulating materials, electrets) [16,26,27], it shows that in conjugated polymers, as expected, far more charge can be accumulated in the presence of an electric field. However, PPY has also a very high charge storage capability, that is, comparable or even higher than that of conventional electret materials [28]. For example, as demonstrated in Fig. 7 (solid line), positive charges with density of about 500 C/m^3 can be stored permanently in the region close to the front electrode. Alternatively, negative poling leads to the storage of negative charges. These pronounced electret properties suggest potential applications of conjugated polymers in the field of electro-acoustical devices and shall therefore be subject to further investigations. However, the build-up of the double charge layer with charges of different signs makes the poling via an electric field less applicable in the framework of electret investigations.

6. Conclusions

In conjugated polymers, space charge can establish when electrons or holes, either brought into the material by injection from the electrodes or redistributed inside the bulk within the external electric field, become trapped at extrinsic or intrinsic defect states. In the first 500 nm near the front electrode of 3–4 μm thick Au/PPYAu devices, we have observed a charged layer with the same sign as the adjacent electrode (homo-charges), whilst deeper inside the sample, at about 1 μm a second layer of opposite charge (hetero-charges) emerges. The first layer is attributed to charge carriers injected from the electrode into trapping sites in the polymer, located near the interface and with an energy deep inside the band gap. The second, hetero-charge layer is ascribed to positive and negative charge arising from extrinsic chemical defects, which separate under the influence of the external field in the bulk of the material and can be trapped, while traversing the trapping zone near the collecting electrode. Poly(2,5-pyridinediyl) as used in our measurements shows pronounced electret properties for both electrons and holes with local charge storage of about 500 C/m^3 near the front electrode. The total trap density has been determined to be about 10^{23} m^{-3}. Because of the double charge layer near the front electrode, the internal electric field is quenched in the bulk of the film, which reduces the effectiveness of the carrier transport within the bulk.

Acknowledgements

The authors express their thanks to the Deutsche Forschungsgemeinschaft and the EPSRC for financial support and U. Weber for technical assistance.

References

[1] Parker ID. J Appl Phys 1994;75:1656–66.
[2] Rikken G, Braun D, Staring EGJ, Demandt R. Appl Phys Lett 1994;65:219–21.
[3] Albrecht U, Bässler H. Chem Phys Lett 1995;235:389–93.
[4] Campbell AJ, Bradley DDC, Lidzey DG. J Appl Phys 1997;82:6326.
[5] Blom PWM, Vissenberg MCJM. Mater Sci Engng 2000;27:53.
[6] Campbell AJ, Weaver MS, Lidzey DG, Bradley DDC. J Appl Phys 1998;84:6737.
[7] Burrows PE, Shen Z, Bulovic V, McCarty DM, Forrest SR, Cronin JA, Thompson ME. J Appl Phys 1996;79:7991.
[8] Campbell AJ, Bradley DDC, Werner E, Brütting W. Synth Met 2000;111–112:273.
[9] Stallinga P, Gomes HL, Rost H, Holmes AB, Harrison MG, Friend RH. Synth Met 2000;111–112.
[10] Campbell IH, Smith DL. Appl Phys Lett 1995;66:3030.
[11] Feller F, Geschke D, Monkman AP. Appl Phys Lett 2001;79:779.
[12] Lang SB, Das-Gupta DK. J Appl Phys 1986;59:2151.
[13] Lang SB. Integr Ferroelectr 1999;27:119.
[14] Leister N, Geschke D. Liq Cryst 1998;24:441.
[15] Bloß P, Steffen M, Schäfer H, Yang G-M, Sessler GM. J Phys D: Appl Phys 1997;30:1668.
[16] Mizutani T. Proc 8th Int Symp Electrets Paris 1994:163.
[17] Dailey S, Halim M, Rebourt E, Horsburgh LE, Samuel IDW, Monkman AP. J Phys: Condens Matter 1998;10:5171–8.
[18] Feller F, Monkman AP. Appl Phys Lett 2000;76:664.
[19] Morozov VA. Methods for solving incorrectly posed problems. Stuttgart: Teubner, 1977.
[20] Groetsch CW. The theory of Tikhonov regularisation for Fredholm equations of the first kind. London: Pitman, 1984.
[21] Honerkamp J, Weese J. Continuum Mech Thermodyn 1990;2:17.
[22] Feller F, Geschke D, Buttgereit R, Roths T, Honerkamp J. Submitted for publication.
[23] Ploss B, Emmerich R, Bauer S. J Appl Phys 1992;72:11.
[24] Ploss B, Bianzano O. Proc 8th Int Symp Electrets Paris 1994:206.
[25] Miyamae T, Yoshimura D, Ishii H, Ouchi Y, Saki K, Miyazaki T, Koike T, Yamamoto T. J Chem Phys 1995;103:2738–44.
[26] Farhat N, Alquie C, Lewiner J. Proc 8th Int Symp Electrets Paris 1994:259.
[27] Suh KS, Kim JE, Oh WJ, Yoon HG. J Appl Phys 2000;87:7333.
[28] Kunstler WI, Gerhard-Multhaupt R. IEEE 1997 annual report. Conference on Electrical Insulation and Dielectric Phenomena, vol. 1; 1997. p. 72.